RAPID COMMUNICATIONS

PHYSICAL REVIEW A VOLUME 50, NUMBER 6 DECEMBER 1994

Non- and nearly hexagonal patterns in sodium vapor generated by single-mirror feedback

T. Ackemann and W. Lange

Institut für Angewandte Physik, Westfälische Wilhelms-Universität Münster, Corrensstraße 2/4, D-48149 Münster, Federal Republic of Germany

(Received 1 July 1994)

In the transmitted beam of a sodium cell with a single feedback mirror highly modulated patterns appear. The patterns possess the dihedral symmetries D_6, D_2, and D_3. More complex patterns consisting of more than one elementary cell show a local hexagonal arrangement. The topological characteristics are very similar to the one of boundary affected patterns predicted in a thin Kerr slice. The instability is due to the competition of diffraction, diffusion, and optical pumping which is influenced by a weak magnetic field. For higher cell-to-mirror distances the observation of an additional length scale indicates a competition between the feedback and a further instability mechanism, probably the counterpropagating beam instability.

PACS number(s): 42.50.Ne, 42.65.-k

The suggestion of d'Alessandro and Firth [1] that in a system consisting of a thin Kerr slice and a single feedback mirror hexagonal patterns form in the transverse directions of the transmitted laser beam is very attractive since it provides an extremely simple example of a pattern-forming system. Corresponding experiments have been performed by means of liquid crystals as the nonlinear medium [2] and in a system based on a liquid crystal light valve [3]. In the latter experiment the influence of an aperture is studied. The results are in agreement with the predictions of a more elaborate theoretical treatment [4] which discusses the influence of boundary conditions. Very recently an experiment involving a cell filled with Rb vapor and feedback by a single mirror has been described [5]. Atomic vapors are attractive in this type of experiment, since they are thought to be free of optical imperfections and moreover they can be described microscopically in principle. The experiment on Rb vapor, however, which was performed without a buffer gas, displayed flowerlike patterns which differ strongly from the predictions of Ref. [4]. One of the possible reasons for the difference may be that a polarization instability was involved which cannot occur in the scalar treatment of [4].

In this paper we describe an experiment employing sodium vapor in a buffer gas atmosphere of fairly high pressure as the nonlinear medium. In this situation the strong homogeneous broadening introduced by the buffer gas facilitates the microscopic description. Moreover, we use circularly polarized light and thus eliminate the possibility of a polarization instability. It should be noted that the system is still very different from the theoretical model of [1] because the medium is by no means thin and cannot be described as a Kerr medium; one of its properties being saturation, another one absorption, and a third one the existence of magneto-optic effects. Yet patterns similar to the one in Ref. [4] are being observed.

In our experiment (cf. Fig. 1) the spatially filtered and expanded beam (the $1/e^2$ radius of irradiance w_0 being 0.84 mm) of a frequency stabilized cw dye laser is injected into a sodium cell. An electro-optic modulator is used for intensity stabilization ($\approx 2\%$) and intensity scanning. The length of the heated zone is 40 mm, the temperature is about 300 °C, which corresponds to an unsaturated Na particle density of about 10^{14} cm^{-3} in a nitrogen buffer gas atmosphere of 300 mbar. We use nitrogen, since it quenches the population of the excited state very efficiently and thus suppresses the trapping of resonance fluorescence [6], which limits the efficiency of optical pumping in an argon buffer gas atmosphere [7]. (In fact, no pattern formation is observed, if nitrogen is replaced by argon.) For reasons discussed below, an external magnetic field is applied which is generated by a system of three pairs of Helmholtz coils. The reflectivity of the feedback mirror is $R = 91.5\%$. The cell center is imaged by a lens onto a charge-coupled-device (CCD) camera. Since we are interested in phenomena of spontaneous symmetry breaking, beam quality is crucial for the experiment. Analysis of the digitized images of the CCD camera shows that the intensity profile of the incoming beam represents very closely a Gaussian distribution and that the beam astigmatism varies around 2% with a standard deviation of 1% (stability against variations of frequency and power during the measurement period). The radius is stable to 4%, the beam pointing to 2% of the beam radius.

At the defocusing side of the D_1 line, dark holes with a modulation depth of up to 100% are found in the image of the near field (Figs. 2 and 3). They occur only in certain ranges of the magnetic field, which is characterized by the

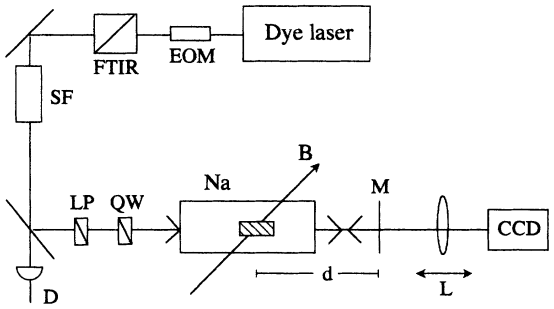

FIG. 1. Experimental setup: EOM, electro-optic modulator; FTIR, variable beam splitter based on frustrated internal reflection; SF, spatial filter; LP, Glan-Thompson polarizer; QW, quarter-wave plate (serving also for optical isolation); M, feedback mirror; L, imaging system; Na, sodium vapor cell; B, magnetic field.

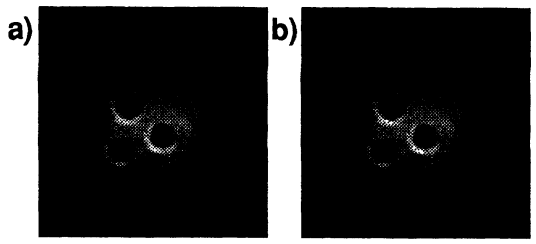

FIG. 2. Examples of patterns typically observed at "low" input power (just above threshold). Parameters: $\vartheta = 296\,^{\circ}\mathrm{C}$, $\Delta = -15$ GHz, $\nu_{tr} = 145$ kHz, $\nu_z = 1140$ kHz. For these particular parameters, the patterns appear if the power is swept adiabatically (0.05 Hz) for (a) down scan, 140–120 mW; (b) up scan, 157–172 mW. The frames have a size of 1.9×1.9 mm^2.

corresponding Larmor frequency, the Landé-factor being $g_F = 0.5$. For a laser detuning of 15 GHz, which gave optimum results, a transverse magnetic field between approximately $\nu_{tr} = 50$ kHz and 180 kHz and a longitudinal one between 700 and 1400 kHz had to be employed. For increasing detuning the necessary magnetic fields decrease (and the particle density has to be increased). In the zero transverse field no patterns occur. The behavior is independent of the sign of the transverse field. In contrast, the patterns appear only for that sign of the longitudinal field component for which light shift and Zeeman shift are opposite. For a lower longitudinal field the patterns discussed so far give way to rings, with a varying modulation of the outermost ring evolving in some cases into flowerlike patterns resembling the one observed in rubidium vapor [5]. Absorption is quite high in this parameter regime; the whole beam transmission is only 10–35 %, while it is 50–90 % for larger longitudinal fields in the regime where hole patterns form.

In general, the observed patterns are stable; only their principal axis fluctuates by a few degrees. The long-term stability depends crucially on the parameter values; e.g., the magnetic field. The patterns can be stable for several minutes or a few tens of minutes, orders of magnitude longer than the characteristic times in the atomic system, which are in the microsecond (period of Larmor precession) and millisecond (diffusion processes) range. For certain parameter combinations they can also show rotations by greater angles or the apparently random alternation back and forth between patterns with different symmetries or between the fully developed hole patterns and distorted roll patterns with a low modulation (not shown). The time scale of these dynamics is of the order of fractions of a second to some tens of seconds. It is still under investigation whether these fluctuations are intrinsic or due to parameter fluctuations.

We will confine ourselves to the hole patterns and first report the results obtained for a short cell-center-to-mirror distance ($d = 76.5$ mm) in more detail. Figure 2 shows the characteristic patterns right above the threshold for symmetry breaking. It consists of three or four holes having D_3 [Fig. 2(a)] or D_2 [Fig. 2(b)] symmetry, respectively. If both patterns are obtained in one power scan, the three-hole pattern appears for lower input power. When the input power is further increased, with the other parameters kept constant, the number of holes grows and a hexagonal [D_6, Fig. 3(a)] or triangular [D_3, Fig. 3(b)] arrangement is observed. At a further increase of power the number of holes continues to grow. The local symmetry is always hexagonal. Mostly no global symmetry exists [Fig. 3(e)], but in narrow parameter regions even fairly complex patterns possess a regular boundary [D_3 symmetry, Fig. 3(d)]. Intermediate patterns [Fig. 3(c)] can be interpreted as hexagons with some additional side lobes, but show some deviations from a pure hexagonal symmetry.

Phenomenologically, it appears that the number of holes increases with increasing beam power simply due to the fact that a larger area of the beam reaches threshold. This seems to show a great similarity to the process of filament formation in other parts of physics, e.g., gas discharge systems [8]. In general, the structural elements tend to group together as close as possible to beam center, so that a transition between patterns with just a few elements (two to six holes) necessarily results in a rearrangement, changing also the symmetry. Thus it is clear that the "weak" boundary conditions provided by the finite beam diameter have an influence on the symmetry of the patterns.

Similar sequences as described above can be obtained if other control parameters (magnetic field, frequency) are varied: At the border of the region of pattern formation, patterns consisting of four or three holes (D_2 or D_3 symmetry) are encountered which evolve into hexagons and more complex patterns with a local hexagonal symmetry. Different types of bistability are observed, i.e., in the up and down scans of parameters a different behavior is found which indicates the coexistence of different stable patterns or of a structured and an unstructured state for one set of parameters.

If the cell-to-mirror distance d is changed between 75 and 175 mm, the log-log plot of the length scale of the patterns versus the mirror distance yields an exponent of 0.51. Surprisingly, it is found that for greater distances ($d = 350$ mm)

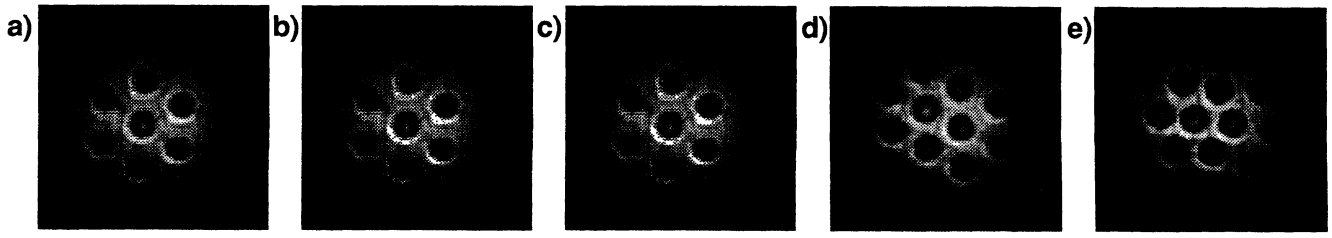

FIG. 3. Examples of patterns typically observed at "high" input power. Parameters as in Fig. 2. (a) Up scan, 172–184 mW; down scan, 152–140; (b) up scan, 184–195 mW; down scan, 181–163 mW; (c) up scan, 200–206 mW; down scan, 196–181 mW; (d) 212 mW; (e) 214 mW (being the maximum available power).

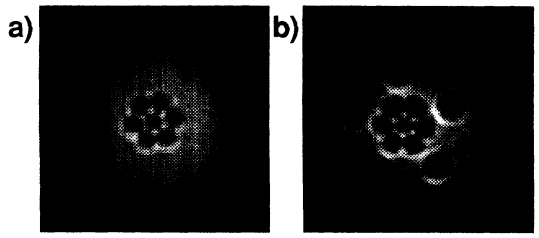

FIG. 4. Patterns observed for larger cell-to-mirror distances. Parameters: $\vartheta \approx 295\,^{\circ}\mathrm{C}$, $\Delta \approx -15$ GHz; (a) $d = 345$ mm, $\nu_{tr} = 41$ kHz, $\nu_z = 1090$ kHz, $P = 155$ mW; (b) $d = 175$ mm, $\nu_{tr} = 72$ kHz, $\nu_z = 987$ kHz, $P = 198$ mW. The frame size is the same as in Figs. 2 and 3.

the patterns have a much smaller scale [Fig. 4(a)] but are otherwise very similar to the ones described before. Especially, the three- and four-hole patterns are also observed. At intermediate distances ($d = 175$ mm) patterns with two length scales are observed [Fig. 4(b)].

The mechanism of the nonlinearity in our experiment is well known. It is based on the creation of orientation in the Na ground state; i.e., it is due to optical pumping between Zeeman sublevels induced by the circularly polarized light. This mechanism necessarily involves absorption, and indeed the small-signal absorption of our sample is on the order of 99%. In a microscopic description, the Na atoms can be regarded as spin-1/2 atoms in good approximation, with the effects of the nuclear spin being neglected [9]. In this description both absorption and dispersion depend linearly on the difference in the population of the two Zeeman sublevels. In the absence of a transverse magnetic field, small intensities of circularly polarized light are sufficient to create the maximum population difference, since the only loss mechanism is provided by wall collisions. Spatial structures, however, are not expected, since they tend to be washed out by diffusion of the fully saturated orientation into the regions of small intensity. For the diffusion constant of sodium atoms in the buffer gas atmosphere ($D \approx 2 \times 10^{-4}$ m^2/s), the diffusion length would equal half of the characteristic length scale $\Lambda \approx 0.25$ mm for a relaxation rate of 13 kHz. Thus a relaxation rate of a few tens of kHz is expected to be necessary to suppress washout [10]. As an alternative, the transverse magnetic field was introduced, which destroys the population difference by inducing spin flips. This process requires degenerate or nearly degenerate Zeeman sublevels. In the present case, however, there is a light shift which is proportional to the local intensity and induces an energy difference between the Zeeman sublevels of a few megahertz in the maxima of intensity. It would restrict the action of the transverse component of the magnetic field to regions of low intensity. The additional longitudinal component of the magnetic field, however, shifts the sites in which spin flips can occur to regions of intermediate intensity and can thus introduce a pronounced spatial dependence of the population difference even in the presence of diffusion, which results in the corresponding spatial dependence of the optical properties. Since transitions occur only in limited spatial regions, a nearly saturated average orientation and a high overall transmission of the sample can be maintained with small laser power.

From these considerations we expect patterns only in nonvanishing transverse fields. The corresponding Larmor frequencies should be in the 100-kHz range. Moreover, we expect that the longitudinal field component can be adjusted to give most efficient pattern formation. (The corresponding Larmor frequency should be in the 1-MHz range.) This should work with one sign of the longitudinal field component only, while the direction of the transverse component is unimportant. By changing the nonlinearity of the medium the magnetic field will also influence the symmetry via the role of the finite beam diameter. All of these predictions are in agreement with the observations. Similar considerations have been used very recently in the interpretation of the magnetic field dependence of a degenerate four-wave-mixing experiment in sodium vapor [11] and have resulted in nearly quantitative agreement ([12]; see also e.g., [13]).

In the plane-wave analysis given in Ref. [1] for the patterns occurring in a thin Kerr slice with a single feedback mirror, the characteristic length of the patterns is

$$\Lambda_n = \sqrt{\frac{2d\lambda}{\frac{3}{2}+2n}} \quad (n = 0,1,\ldots). \tag{1}$$

This fits with the scaling law found in the experiment for small distances d, and it also fits reasonably with the absolute values being observed, if $n = 0$. In a diffusive medium the threshold increases with n, and thus the observation of narrow structures is not expected in the absence of larger ones. In the case of a Gaussian beam, however, the boundary conditions come into play. For $d = 350$ mm the ratio between the beam radius and the value of Λ_0 obtained from Eq. (1) is $\eta = 1.62$, while the smallest value of η reported in Ref. [4] is 1.8. Thus it should not be too surprising that the corresponding structure is not observed. It is expected, however, that the $n = 0$ instability will be replaced by the one with $n = 1$, and so on, and this is not found in the experiment: the small scale structure would require $n = 3$ in Fig. 4.

On the other hand it has to be kept in mind that the experiment is by no means performed in a thin medium, but the zone filled with atomic vapor has a finite length ($L = 40$ mm). Instabilities which do not require a feedback mirror but arise from the interaction of counterpropagating beams may occur in this situation (see, e.g., Ref. [14]). Their characteristic length does not depend on the cell-to-mirror distance, of course, just as the unidentified small scale structures in our experiment. Its value $\sqrt{2L\lambda}$ [1] obtained in a plane-wave analysis is within 25% of the one in the observed small scale structure. Therefore we suppose that in the experiment there is a competition between the single-mirror instability and the instability occurring in counterpropagating beams. For small distances d the former wins, possibly due to its larger length scale, while it is disfavored for large d due to the boundary effects provided by the finite beam width. At intermediate distances d both types of pattern-forming mechanisms seem to operate simultaneously.

Note added. After the submission of the paper the observation of dihedral patterns in a liquid crystal cell with a Kerr-like nonlinearity was reported [15].

We thank M. Möller for useful discussions.

[1] G. d'Alessandro and W. J. Firth, Phys. Rev. A **46**, 537 (1992).
[2] R. Macdonald and H. J. Eichler, Opt. Commun. **89**, 289 (1992); M. Tamburrini, M. Bonavita, S. Wabnitz, and E. Santamato, Opt. Lett. **18**, 855 (1993).
[3] E. Pampaloni, S. Residori, and F. T. Arecchi, Europhys. Lett. **24**, 647 (1993).
[4] F. Papoff, G. D'Alessandro, G. L. Oppo, and W. J. Firth, Phys. Rev. A **48**, 634 (1993).
[5] G. Grynberg, A. Maître, and A. Petrossian, Phys. Rev. Lett. **72**, 2379 (1994).
[6] M. Schiffer, G. Ankerhold, E. Cruse, and W. Lange, Phys. Rev. A **49**, R1558 (1994).
[7] G. Ankerhold, M. Schiffer, D. Mutschall, T. Scholz, and W. Lange, Phys. Rev. A **48**, R4031 (1993).
[8] K. G. Müller, Phys. Rev. A **37**, 4836 (1988).
[9] M. W. Hamilton, W. J. Sandle, J. T. Chilwell, J. S. Satchell, and D. M. Warrington, Opt. Commun. **48**, 190 (1983); M. Möller and W. Lange, Phys. Rev. A **49**, 4161 (1994).
[10] A more detailed treatment based on Eqs. (7) and (8) of [1] yields the possibility of pattern formation in the range of 5–100 kHz.
[11] M. Schiffer, E. Cruse, and W. Lange, Phys. Rev. A **49**, R3178 (1994).
[12] An additional effect of the magnetic field, the breaking of the rotational symmetry by the transverse magnetic field, appears to be not significant since the induced lateral displacements are rather small [13], and it is experimentally checked that the axis of the observed patterns does not depend on the direction of the transverse field.
[13] T. Blasberg and D. Suter, Phys. Rev. Lett. **69**, 2507 (1992).
[14] A. Petrossian, M. Pinard, A. Maître, J. Y. Courtois, and G. Grynberg, Europhys. Lett. **18**, 689 (1992).
[15] E. Ciamarella, M. Tamburrini, and E. Santamato, Phys. Rev. A **50**, R10 (1994).

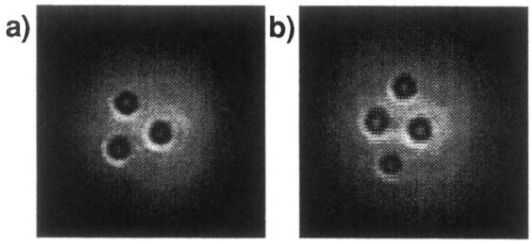

FIG. 2. Examples of patterns typically observed at "low" input power (just above threshold). Parameters: $\vartheta = 296\,^{\circ}\mathrm{C}$, $\Delta = -15$ GHz, $\nu_{tr} = 145$ kHz, $\nu_z = 1140$ kHz. For these particular parameters, the patterns appear if the power is swept adiabatically (0.05 Hz) for (a) down scan, 140–120 mW; (b) up scan, 157–172 mW. The frames have a size of 1.9×1.9 mm^2.

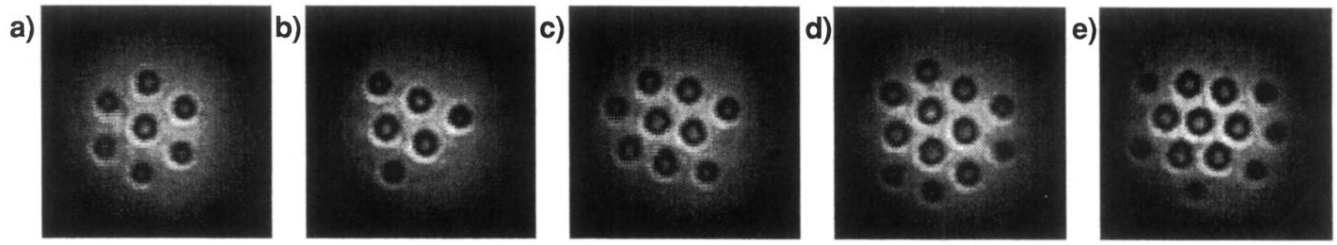

FIG. 3. Examples of patterns typically observed at "high" input power. Parameters as in Fig. 2. (a) Up scan, 172–184 mW; down scan, 152–140; (b) up scan, 184–195 mW; down scan, 181–163 mW; (c) up scan, 200–206 mW; down scan, 196–181 mW; (d) 212 mW; (e) 214 mW (being the maximum available power).

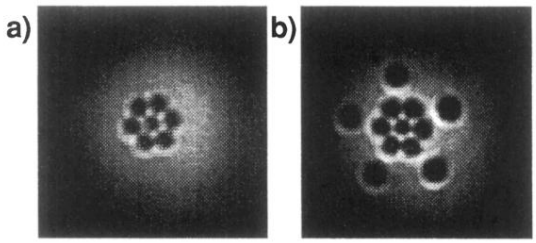

FIG. 4. Patterns observed for larger cell-to-mirror distances. Parameters: $\vartheta \approx 295\,^{\circ}\mathrm{C}$, $\Delta \approx -15$ GHz; (a) $d = 345$ mm, $\nu_{tr} = 41$ kHz, $\nu_z = 1090$ kHz, $P = 155$ mW; (b) $d = 175$ mm, $\nu_{tr} = 72$ kHz, $\nu_z = 987$ kHz, $P = 198$ mW. The frame size is the same as in Figs. 2 and 3.